Structure of tert-Butyl Alcohol−Water Mixtures Studied by the RISM Theory

ARTICLE *in* THE JOURNAL OF PHYSICAL CHEMISTRY B · APRIL 2002

Impact Factor: 3.3 · DOI: 10.1021/jp013400x

2 AUTHORS:

Koji Yoshida
Fukuoka University
62 PUBLICATIONS **684** CITATIONS
SEE PROFILE

Toshio Yamaguchi
Fukuoka University
203 PUBLICATIONS **3,795** CITATIONS
SEE PROFILE

Structure of *tert*-Butyl Alcohol−Water Mixtures Studied by the RISM Theory

Koji Yoshida and Toshio Yamaguchi

Department of Chemistry, Faculty of Science, Fukuoka University, Jonan-ku, Fukuoka 814-0180

Andriy Kovalenko and Fumio Hirata*

Institute for Molecular Science, Myodaiji, Okazaki 444−8585

Received: September 5, 2001; In Final Form: February 8, 2002

We calculated the site−site radial distribution functions for binary mixtures of *tert*-butyl alcohol (TBA) and water over the whole range of TBA molar fraction. The description uses the reference interaction site model (RISM) integral equation theory in the dielectrically consistent approach of Perkyns and Pettitt (DRISM), and the closure approximation of Kovalenko and Hirata (KH) providing appropriate description for association of polar molecular species of density ranging from gas to liquid. We employed the extended simple point charge (SPC/E) model for water, and the optimized potential for liquid simulations (OPLS) force field for TBA. The partial radial distribution functions obtained for the TBA−water mixture are in qualitative agreement with those available from neutron diffraction experiments and molecular dynamics simulations. It is found that hydrogen bonds between all species are enhanced with rise of the TBA concentration. The tetrahedral-like network of hydrogen bonding in dilute TBA aqueous solution gradually turns into the zigzag-like structure for a high TBA concentration. In dilute aqueous solution, TBA molecules cluster by the hydrophobic methyl groups, whereas their hydroxyl groups are incorporated into the water hydrogen-bonding cage surrounding the TBA aggregate. In concentrated TBA, water as well as TBA molecules associate into the zigzag-like hydrogen-bonding chains. The present work shows that the RISM/KH theory is able to qualitatively predict the association structure of alcohol−water liquid mixtures.

Introduction

Aqueous solutions of alcohols have long been used as solvents in chemical synthesis, liquid chromatography, solvent extraction, etc. in view of their characteristic properties meeting industrial needs.[1] Because alcohols are amphiphilic molecules possessing both alkyl and hydroxyl groups, they have features such as anomalies in the thermodynamic quantities originating from a subtle balance between the hydrophobic and hydrophilic interactions of alcohol and water molecules in solution. Much attention has also been generated from bioscience to the amphiphilic nature of alcohols as solvents assisting protein denaturation due to the promotion of the α-helix structure of peptides and proteins. Recently, X-ray diffraction and mass spectroscopy were used to reveal the miscroscopic structure of aqueous solutions of methanol[2] and ethanol,[3,4] and to find a composition of clusters predominant in the solutions. It was found that a structural transition of the clusters is responsible for the anomalies in the thermodynamic properties. Furthermore, dynamic light scattering and small-angle X-ray and neutron diffraction investigations of micelle formation and protein denaturation in aqueous solutions of ethanol have shown that the size of micelles and the transition from the β-sheet to α-helix conformation correlate well with the microscopic structure of the solvents.[5] Similar findings have been reported for micellization and protein folding in aqueous solutions of ethanol and *tert*-butyl alcohol from calorimetric studies.[6] Thus, a detailed investigation at the molecular level is essential to understand mechanisms underlying various unique chemistry, physics, and bioscience phenomena observed in alcohol−water solutions as well as to predict their macroscopic characteristics.

Among monohydroxyl alcohols that are miscible with water in any proportion, *tert*-butyl alcohol (TBA) possesses the biggest alkyl group and hence exhibits the largest hydrophobic effect. The TBA−water mixture is characterized by such anomalies as, for instance, a sharp minimum of the partial molar volume[7] and a maximum of the partial molar specific heat[8] at TBA molar fraction $X_{TBA} \sim 0.04$. Small-angle X-ray diffraction[9,10] and neutron scattering[11] experiments showed that the density fluctuations of the TBA solution in the molar fraction range $X_{TBA} \sim 0.06-0.16$ are largest among aqueous solutions of monohydroxyl alcohols. It was concluded that the characteristic factor determining the mixing state of aqueous solution of TBA at these concentrations is the formation of the cage structure of water molecules around a TBA, such as clathrate−hydrate-like structure.[9,10] Very recent infrared studies of TBA in aqueous solution[12] revealed the change in the water OH and alkyl CH stretching bands with a rise of the TBA molar fraction. As it exceeds a critical concentration $X_{TBA} \sim 0.025$, the CH stretching band maximum frequency (constant for smaller X_{TBA}) starts falling, which is indicative of the depletion of the aqueous environment around the TBA methyl groups. This behavior can be linked to a progressive hydrophobic clustering of the TBA molecules above the critical concentration.[12,13]

Nakanishi and co-workers carried out Monte Carlo (MC) and molecular dynamics (MD) simulations of dilute aqueous solution represented with 1 TBA + 215 water molecules,[14] and of 0.03 mole fraction TBA in water.[15] They reported for the first time that, as compared to the hydration of methanol, the water

* Corresponding author. Fax: +81 (564) 53-4660. E-mail: hirata@ims.ac.jp.

10.1021/jp013400x CCC: $22.00
Published on Web 04/19/2002

structure around a TBA molecule is more pronounced and association of TBA occurs even in dilute solutions. Kusalik et al.[16] recently performed MD simulation studies on 0.02 and 0.08 mole fraction TBA aqueous solutions as well as on pure TBA. They found that small aggregates of a few alcohol molecules in tail-to-tail pairwise arrangements are formed in the 0.08 mole fraction TBA solution, with no evidence for hydrogen bonding between the alcohol molecules. However, the tendency of TBA clustering appeared only slightly in the 0.02 mole fraction TBA solution. It is not clear whether the MD result for TBA aggregation is statistically significant given the small number of solutes present in their numerical representation of this dilute system.

Bowron, Finney, and Soper made neutron diffraction (ND) experiments with H/D isotopic substitution on seven different samples of aqueous TBA solutions[17] at the 0.06, 0.11, and 0.16 mole fractions of TBA as well as on pure TBA liquid.[18] The ND data were processed by the empirical potential structure refinement (EPSR) method of Soper.[19] It assumes the site−site intermolecular interaction potentials of the system and then adjusts them to fit the partial distribution functions repeatedly obtained by a Monte Carlo simulation with these potentials to the experimental data. The EPSR modeling method ensures correct statistical uncertainties of the site−site distribution functions,[19] and significantly reduces noise initially present in the ND data.[17,18] The intermolecular orientational correlations between solute alcohol molecules were analyzed in terms of spherical harmonics, showing the dependences on particular angles of the molecular orientation with averaging over the remaining angles. The EPSR results demonstrated that the majority of association of the TBA molecules is through their nonpolar methyl group regions rather than via hydrogen-bonding interactions between their polar hydroxyl groups. Evidence for hydrogen bonding between the alcohol molecules in the solution over the investigated concentration range was absent, even in the 0.16 mole fraction of TBA. Furthermore, the deduced quantity of water molecules around a TBA aggregate was sufficient to satisfy the expected hydrogen-bonding requirements of the TBA hydroxyl groups. One should note that an inherent limitation of this treatment consists of the fact that, in dilute solution, the structural information about the solute may have significant uncertainties because of its small contribution to the neutron scattering intensities.

Among theoretical approaches, advantageous is integral equation method which operates in the thermodynamic limit and thus yields the solution structure free from statistical error at any dilution. Successful description for realistic models of molecular liquids is provided by the reference interaction site model (RISM) integral equation theory.[20] It was first developed by Chandler and Andersen[21,22] for nonpolar molecular liquids. By adapting the hypernetted chain (HNC) closure to the RISM integral equations, Hirata et al extended the theory to polar solvents[23] and various complex ion-molecular systems.[24] Perkyns and Pettitt[25] elaborated the dielectrically consistent RISM theory (DRISM) involving bridge corrections to the HNC closure to ensure the empirical values of the calculated dielectric constant as well as consistency of the static dielectric properties for electrolyte solutions. Kovalenko and Hirata proposed the closure approximation[26,27] (below referred to as KH) which enables the RISM description for association of polar molecular fluids in a wide density range from gas to liquid.[27] Tanaka, Walsh, and Gubbins[28] employed the RISM/HNC theory to study methanol−water mixtures. To our knowledge, the RISM approach has not been applied to higher alcohols−water mixtures. In the present study, we perform the DRISM/KH calculations for aqueous solutions of TBA in the whole range of concentration. We make a comparison between the partial distribution functions obtained and the recent neutron diffraction data processed by the EPSR method.[17,18] We conclude on the structure modification of the TBA−water system with the rise of the TBA molar fraction.

Methods

RISM Theory. The RISM integral equations are written in the matrix form as[20−22]

$$\mathbf{h} = \mathbf{w} * \mathbf{c} * \mathbf{w} + \mathbf{w} * \mathbf{c} * \boldsymbol{\rho} * \mathbf{h} \tag{1}$$

where **h** and **c** are respectively the matrixes of the *intermolecular* total and direct correlation functions $h_{\alpha\gamma}(r)$ and $c_{\alpha\gamma}(r)$ between interaction sites α and γ of different molecules, $\mathbf{w} = \delta(r - l_{\alpha\gamma})/(4\pi l_{\alpha\gamma}^2)$ is the *intramolecular* matrix specifying the geometry of species with site separations $l_{\alpha\gamma}$ in a molecule (implying $l_{\alpha\alpha} = 0$), $\rho = \delta_{\alpha\gamma}\rho_\alpha$ is the diagonal matrix comprising the number densities of sites, and "*" means convolution in the direct space and summation over repeating indices. The size of each matrix is determined by the total number of distinct interaction sites in all the molecular species. The site−site radial distribution functions (RDFs), $g_{\alpha\gamma}(r) = h_{\alpha\gamma}(r) + 1$, can be compared with the results of computer simulations as well as X-ray and neutron diffraction experiments.

In this study, we complement the RISM integral eq 1 with the KH closure approximation[26,27] which reads for the site−site correlations as

$$\begin{aligned} g_{\alpha\gamma}(r) &= \exp(d_{\alpha\gamma}(r)) \quad \text{for} \quad d_{\alpha\gamma}(r) < 0 \\ &= 1 + d_{\alpha\gamma}(r) \quad \text{for} \quad d_{\alpha\gamma}(r) \geq 0 \end{aligned} \tag{2a}$$

$$d_{\alpha\gamma}(r) = -u_{\alpha\gamma}(r)/(k_B T) + u_{\alpha\gamma}(r) - u_{\alpha\gamma}(r) + b_{\alpha\gamma}(r) \tag{2b}$$

where $u_{\alpha\gamma}(r)$ is the site−site interaction potential between molecules, scaled by the Boltzmann constant k_B times temperature T. It combines the HNC approximation for the regions of density profile depletion, $g_{\alpha\gamma}(r) < 1$, with exponent linearization reducing to the mean spherical approximation (MSA) for the regions of enrichment, $g_{\alpha\gamma}(r) > 1$. This mixed scheme provides appropriate description for long-range enhancement tails of critical regime and high peaks of association in molecular fluids. The bare MSA, although appropriate to critical phenomena, often produces unphysical regions of negative distribution functions, whereas the HNC closure becomes divergent at concentrations corresponding to enhanced clustering, in particular in molecular associating liquids. At the same time, it was shown[26] that the partial linearization (2a) does not affect the structure of ambient water significantly as compared to the common HNC closure. The first peak of the oxygen−oxygen distribution, for instance, gets somewhat lower but wider, and so both the KH and HNC closures to the RISM equations yield very similar results for the coordination numbers of the ambient water. Besides the KH approximation, the closure (2) also includes the consistent dielectric bridge correction $b_{\alpha\gamma}(r)$ analogous to that in the DRISM approach of Perkyns and Pettitt[25] enforcing the experimental magnitude of the dielectric constant of the solution.

Models of Water and TBA. In the calculations, the temperature is set equal to 298 K. The densities and dielectric constants of the solution at the given molar fractions are taken from the experimental data for TBA−water mixtures.[29,30] The intermolecular interaction potentials comprise pairwise site−site con-

TABLE 1: Parameters of the Water and TBA Models

Water			
bond	r/Å	angle	θ/deg
O_W-H_W	1.000	$H_W-O_W-H_W$	109.5
atoms	q/e	σ/Å	ϵ/kcal/mol
O_W	−0.8476	3.166	0.1554
H_W	0.4238	1.000	0.0460

TBA			
bonds	r/Å	angles	θ/deg
C_C-C	1.530	$C-C_C-C$	108.0
C_C-O	1.430	$C-C_C-O$	112.0
$O-H$	0.948	C_C-O-H	108.5
atoms	q/e	σ/Å	ϵ/kcal/mol
C (methyl group)	0.000	3.960	0.145
C_C	0.265	3.800	0.050
O	−0.700	3.070	0.170
H	0.435	1.000	0.046

tributions $u_{\alpha\gamma}(r)$ represented by the Coulomb and 12−6 Lennard-Jones terms,

$$u_{\alpha\gamma}(r) = \frac{q_\alpha q_\gamma}{r} + 4\epsilon_{\alpha\gamma}\left[\left(\frac{\sigma_{\alpha\gamma}}{r}\right)^{12} - \left(\frac{\sigma_{\alpha\gamma}}{r}\right)^{6}\right] \qquad (3)$$

where q_α is the electric charge of site α, and $\sigma_{\alpha\gamma}$ and $\epsilon_{\alpha\gamma}$ are respectively the Lennard-Jones size and energy parameters for interaction sites pair $\alpha\gamma$. The cross terms for unlike sites $\alpha\neq\gamma$ are determined by the standard Lorentz−Berthelot mixing rules, $\sigma_{\alpha\gamma} = (\sigma_{\alpha\alpha}+\sigma_{\gamma\gamma})/2$ and $\epsilon_{\alpha\gamma} = (\epsilon_{\alpha\alpha}\epsilon_{\gamma\gamma})^{1/2}$.

For water, we employed the extended simple point charge (SPC/E) model.[31] The only difference is that a Lennard-Jones size of 1 Å is introduced for the water hydrogen sites. It does not affect the entire potential of the water molecule since the hydrogens are situated well inside the oxygen repulsive core, and the hydrogen cores so introduced coincide with the edge of the oxygen one. This adjustable parameter of the RISM theory allows one to optimize the description for hydrogen bonds.[32,33] The same size is assigned to the hydrogen site in the TBA hydroxyl group. The potential parameters of the TBA molecule are taken from the united-atom OPLS force field.[34] The UA-OPLS model of TBA has a positive charge on the hydroxyl hydrogen of TBA, and a negative charge on the hydroxyl oxygen. The methyl carbons are neutral. The TBA electroneutrality is attained by the positive charge of the central carbon. The methyl groups of TBA are treated as united atoms. The molecular geometry, site charges, and Lennard-Jones parameters of water and TBA molecules are summarized in Table 1.

Choosing the TBA model, we aim for qualitative recapitulation of the TBA−water solvation structure modification with the TBA molar fraction found in experiment and molecular simulations, rather than for quantitative agreement with the numerical data available. The 6-site united-atom model of TBA is substantially better than the "double"-simplified model regarding the whole *tert*-butyl group $C(CH_3)_3$ as a united atom.[16] The latter considerably distorts the overall toroidal shape of the bulky hydrophobic group. On the other hand, the united-atom simplification only for the TBA methyl groups does not sacrifice, in our opinion, the significant features of the TBA−water solution structure, although some details of the methyl−methyl RDFs are obviously lost. In the all-atom TBA models,[16−18] the methyl hydrogens are situated well inside the methyl carbon core and their charges are quite small and almost neutralized with the carbon one. Therefore, the 6-site OPLS model of TBA represents the shape of its hydrophobic group quite well, which is important to account for the balance between the hydrophobic and hydrophilic interactions in the TBA−water mixture. The use of an all-atom TBA model would be of significant benefit, provided the site parameters are adjusted to represent the potential change in a TBA−water mixture of a given composition, similarly to potential modification in the EPSR modeling.[16] This goes beyond the scope of the present work.

Numerical Solution. The DRISM/KH integral eqs 1−2 have been discretized on an exponentially spaced nonlinear radial grid of 512 nodes with the lower and upper limits $r_{min} = 0.0166$ Å and $r_{max} = 587$ Å to calculate the convolution in eq 1 by means of the nonlinear radial fast Fourier transform.[35,36] The forward and backward Fourier transforms of the long-range asymptotics of the site−site total and direct correlation functions $h_{\alpha\gamma}(r)$ and $c_{\alpha\gamma}(r)$ due to the electrostatic interactions are evaluated analytically as described in ref 37, while the grid size is overwhelmingly large to handle the remaining shorter range components of $h_{\alpha\gamma}(r)$ and $c_{\alpha\gamma}(r)$. Further increase of the maximal distance r_{max} as well as grid resolution does not improve the precision of the results. The equations have been converged to the root-mean-square accuracy of 10^{-6} by means of the method of modified direct inversion in the iterative subspace (MDIIS).[38,39] It ensures great acceleration and stability of convergence.

Results and Discussion

The features of all the site−site RDFs we have calculated fall into the consistent picture for the structure of the TBA−water mixture, and illustrate its change with the TBA concentration. They are in qualitative agreement with the results of neutron diffraction (ND) experiments of Bowron, Finney, and Soper for TBA−water solutions[17] and pure TBA.[18] Our results in general comply also with the molecular dynamics (MD) simulations of Kusalik et al.[16] for TBA in the pure liquid and aqueous solution, available at present. However, the latter use the site charges and Lennard-Jones parameters of the all-atom TBA potential model considerably different from the OPLS force field. This hinders direct quantitative comparison since the results were found to be sensitive to the choice of potential models.[16−18]

Plots of Figure 1 present the changes in the site−site RDFs $g_{\alpha\gamma}(r)$ obtained for the TBA−water mixture with the TBA molar fraction X_{TBA} varying in the whole range from infinite dilution in pure water ($X_{TBA} \rightarrow 0$) to pure TBA ($X_{TBA} \rightarrow 1$). The molecular interaction sites are labeled as follows: C_C means TBA central carbon; C, TBA methyl group carbon; O, TBA hydroxyl group oxygen; H, TBA hydroxyl group hydrogen; O_W, water molecule oxygen; O_H, water molecule hydrogen. Figure 2 makes a comparison with the ND/EPSR results[17,18] at similar values of X_{TBA} for the C_C-C_C, C_C-O, and C_C-H correlations between the TBA hydrophobic and hydroxyl groups, illustrative of the hydrogen-bonding changes. The experimental curves at successive X_{TBA} are spaced apart because of their statistical noise confusing the view. For the other partial RDFs obtained in ND/EPSR experiment, we refer the reader to refs 17 and 18. Figure 3 shows the differences between the hydrogen-bonding structures of the TBA−water mixture in the two limiting cases of TBA and water at infinite dilution, manifesting in the hydrogen−hydrogen correlations. The major modification of the TBA−water solution structure with rise of the TBA molar fraction consists in gradual transition from the tetrahedral-like hydrogen-bonding network typical of water to the zigzag hydrogen-bonding structure peculiar to alcohol. In dilute TBA solutions, the hydroxyl group of a TBA molecule is included into the water

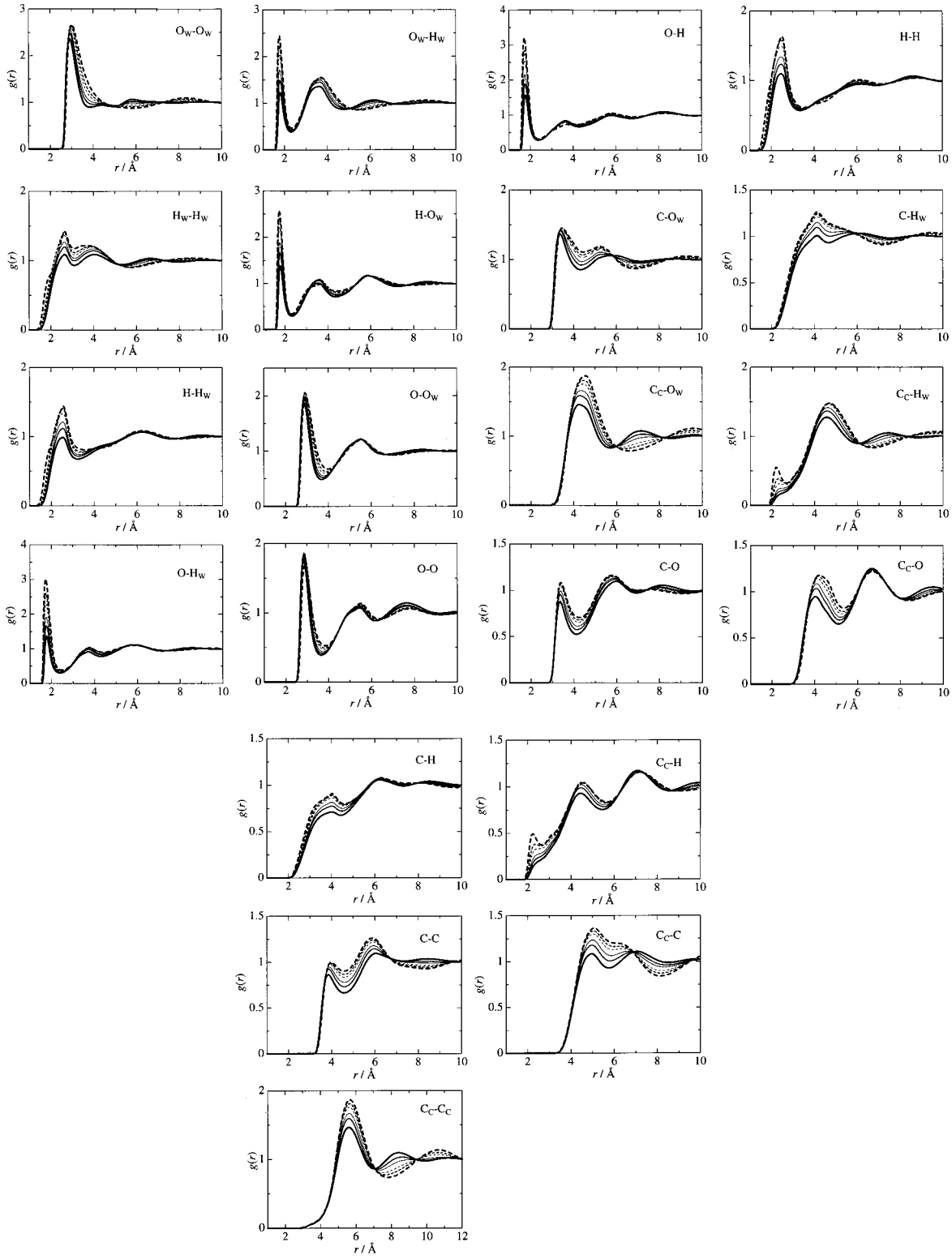

Figure 1. Intermolecular site−site radial distribution functions of *tert*-butyl alcohol−water solution, following from the DRISM/KH theory. TBA molar fractions: 0, 0.1, 0.2, 0.4, 0.6, and 1 (bold solid, normal solid, thin solid, and thin short-dashed, normal short-dashed, bold short-dashed lines, respectively).

tetrahedral-like hydrogen-bonding network forming a cage around the TBA hydrophobic *tert*-butyl group. With rise of the TBA concentration in dilute aqueous solution, TBA molecules progressively cluster by the *tert*-butyl groups due to their hydrophobic attraction in water, while the TBA hydroxyl groups remain included into the hydrogen-bonding cage of water around the whole TBA aggregate. As follows from the below analysis of the TBA−TBA correlations, zigzag hydrogen-bonding chains arise in aqueous TBA beginning from the molar fraction $X_{TBA} > 0.2$ and take over in concentrated TBA solution for approximately $X_{TBA} > 0.4$. Water molecules in concentrated TBA are incorporated into the alcohol hydrogen-bonding zigzag structure. Figures 4 and 5 exemplify typical configurations in the solution at infinite dilution of TBA and infinite dilution of water, respectively. We emphasize that these configurations should be regarded as "snapshots" of fluctuating molecular

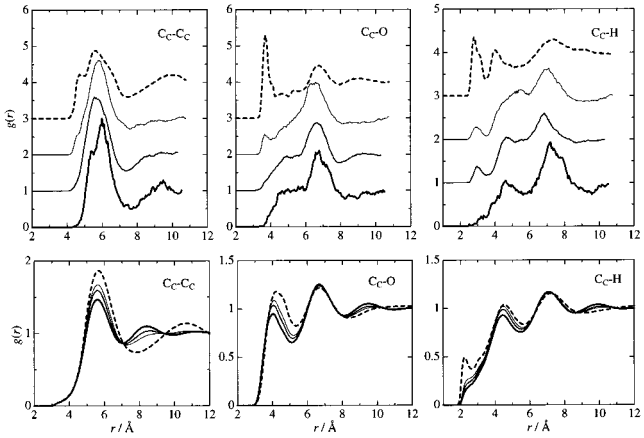

Figure 2. Change of the intermolecular radial distribution functions with the TBA concentration X_{TBA}, following from the DRISM/KH theory against the ND experiment data processed with EPSR modeling.[17,18] Distributions between TBA central carbons (C_C-C_C), and between TBA central carbon and TBA hydroxyl group oxygen and hydrogen (C_C-O and C_C-H). DRISM/KH results for $X_{TBA} = 0$, 0.1, 0.2, and 1 (bold solid, normal solid, thin solid, and bold short-dashed lines, respectively), and ND/EPSR data for $X_{TBA} = 0.06$, 0.11, 0.16, and 1 (same lines sequence in ascending order of X_{TBA}).

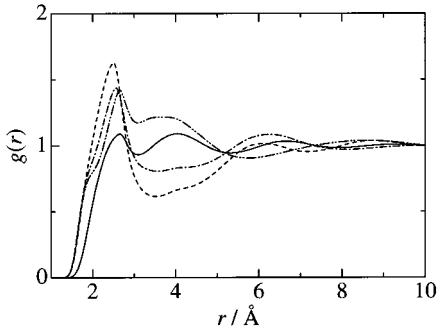

Figure 3. Comparison of the intermolecular radial distribution functions between hydroxyl hydrogens in *tert*-butyl alcohol−water solution, following from the DRISM/KH theory. H_W-H_W of pure water (solid line), H−H of pure TBA (long-dash line), and H−H_W and H_W−H_W for water at infinite dilution in pure TBA (dash−dotted and dash-double dotted line, respectively).

coordinates and hydrogen bonds. Hydrogen-bonding structure is not permanent; it is breaking, reforming, and exchanging molecules within thermal fluctuations. In this context, cartoons of Figures 4 and 5 represent the most probable arrangements of the fluctuating solution species, but not a steady chemical structure with well-defined bonds or long chains.

Correlations between Water and TBA Hydroxyl Groups. The first peak of the O_W-O_W RDF at 2.8 Å corresponding to first-neighboring water molecules becomes higher and wider with rise of the TBA concentration. The feature at 4.5 Å representing the tetrahedral-like ordering of water due to the hydrogen bonding considerably diminishes at $X_{TBA} > 0.1$, which shows that the tetrahedral-like water structure is disrupted at the higher TBA molar fractions. The evolution of the hydrogen bonding against the TBA molar fraction in the solution is seen in the O_W-H_W RDF. Its first peak becomes higher with rise of the TBA concentration. A similar behavior is observed in the O−H_W, H−O_W, and O−H RDFs. Their second as well as first peaks get higher. In concentrated TBA solution, the first peaks of the H_W-H_W, H−H_W, and H−H RDFs increase too. In the ND experiment,[17] all the corresponding peaks increase as the TBA concentration rises. The second peaks of the H_W-H_W and H−H RDFs increase with rise of the TBA concentration whereas

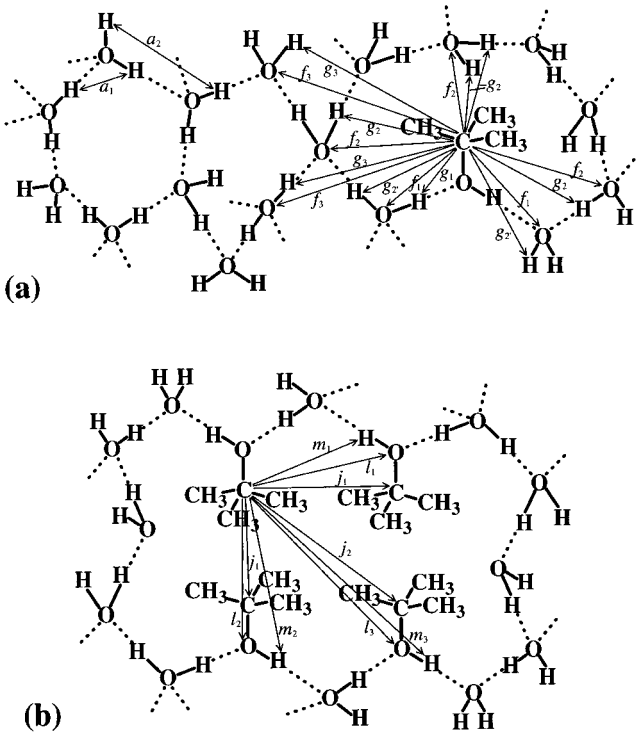

Figure 4. Schematic representation of tetrahedral-like configurations of hydrogen bonding in *tert*-butyl alcohol−water solution at infinite dilution of TBA. (a) TBA molecule in water, and (b) association of dilute TBA in water.

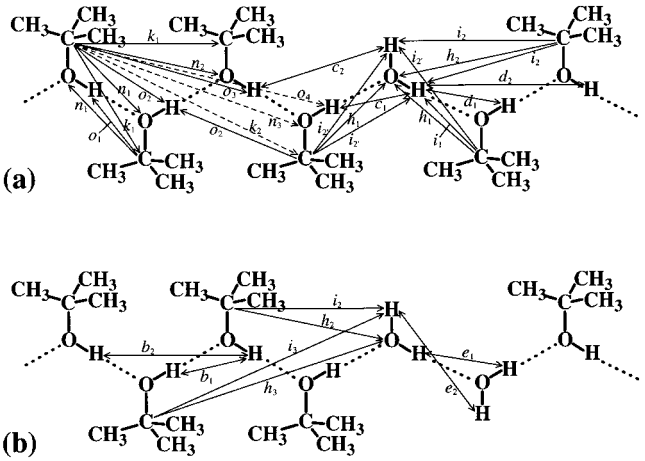

Figure 5. Schematic representation of zigzag-like configurations of hydrogen bonding in *tert*-butyl alcohol−water solution at infinite dilution of water. (a) Water molecule in TBA, and (b) association of dilute water in TBA.

that of H−H_W is not affected much, which also complies with the ND results.[17] These findings indicate that the water−water, TBA−water, and TBA−TBA hydrogen bonds strengthen with rise of the TBA molar fraction, in qualitative agreement with the MD results[12] as well as ND data.[17] This is reasonable since two hydrogens are bonded with a hydroxyl oxygen in the tetrahedral-like structure and only one hydrogen in the zigzag hydrogen-bonding structure. In the latter, the oxygen charge is thus less screened by the hydrogen-bonded hydrogens, which results in stronger hydrogen bonding for every pair of the solution species entering the alcohol-type zigzag hydrogen-bonding structure. The transition of the water hydrogen bonding from the tetrahedral-like to zigzag structure with the gradual change from pure water to pure TBA is evident from the shifts of the O_W-O_W RDF peak at 5.8 to 8.5 Å, of the third O_W-H_W

peak from 6.2 to 8.5 Å, and of the third H_W-H_W peak from 6.6 to 8.7 Å.

The height of the first peak in the $O-H_W$ RDF is almost equal to that in the $H-O_W$ RDF. This implies that the hydroxyl group of TBA works as a donor as well as acceptor to form hydrogen bonds between water and TBA symmetrically. On the contrary, the ND data[17] indicate that the hydroxyl group of TBA is a noticeably stronger hydrogen bond acceptor than a donor to water. Assuming that the ND experiment resolves the above-mentioned peaks with enough confidence, this disagreement might be a drawback of the present potential models with fixed site charges and rigid geometry of the water and TBA molecules, which are optimized for pure water and TBA liquids. In the mixture, however, they can be subject to considerable change, which is accounted for in the EPSR procedure by adjusting the intermolecular potentials to best fit the experiment. It should be noted that the hydrogen-bonding peak position in the RISM prediction is somewhat shifted to a smaller distance as compared to the experiment. This is caused by the well-documented artifact of the RISM theory in treatment of so-called auxiliary sites.[20] However, it is not crucial since relative changes in the peak position and height are more important for the analysis of the system structure.

A shoulder on the ascending slope of the first peak of the $H-H_W$ as well as H_W-H_W RDFs emerge at the 0.16 mole fraction of TBA in the ND results of Bowron et al.[17] They suggested it might be an artifact because of a small number of water molecules in the simulation box. However, we have observed a similar feature arising in the H_W-H_W and $H-H_W$ RDFs at the higher TBA concentrations, whereas the RISM theory operates in the thermodynamic limit and the discretization grid resolution and size are sufficiently large to render the solutions practically size independent. Figure 3 draws a comparison of the H_W-H_W and $H-H_W$ RDFs having shoulders at infinite dilution of water in TBA, with the H_W-H_W of pure water and H−H of pure TBA. The corresponding hydrogen-bonding structures are schematically depicted in Figures 4 and 5. Notice the following two differences between the H_W-H_W RDF characteristic of the tetrahedral-like hydrogen bonding network in pure water and the H−H RDF peculiar to the zigzag hydrogen bonding in pure TBA. The first peak of the latter (corresponding to distance b_1 in Figure 5b) is significantly higher and wider than that of the former (corresponding to a_1 in Figure 4a). While the peak maximum of the latter is shifted to a shorter distance with respect to that of the former by 0.15 Å, the difference between the ascending slopes of the peaks is 0.25 to 0.45 Å. Since the O−H first peak describing the hydrogen-bonding distance is very narrow, the wider H−H first peak corresponds to a wider, less directed angular distribution of hydrogen bonds in the alcohol zigzag as compared to tetrahedral-like water hydrogen-bonding structure. This is obviously related to the difference of the interaction potentials of water and alcohol. The screening of the negative hydroxyl O by the positive charges of the hydroxyl H and more distant C_C in the TBA molecule is weaker than that by two hydrogens in the water molecule. Next, the second peak of H_W-H_W in pure water at 4 Å corresponds to the two distant hydrogens in a hydrogen-bonded pair of waters (a_2 in Figure 4a), and its third peak at 6.6 Å is between farther neighbors in the tetrahedral-like structure of water. As distinct, the H−H RDF in pure TBA has only a small hump in a valley at 4 Å, whereas its second peak at 6 Å gives the H−H separation between the second nearest neighbors in the zigzag hydrogen-bonding chain of TBA (b_2 in Figure 5b). These differences are also evident in the MD simulation[16] and ND experiment[17] data. The above features seen in Figure 3 suggest the following interpretation for the first peak shoulders on the H_W-H_W and $H-H_W$ RDFs in concentrated TBA. The angular distribution of the hydrogen bond between a TBA hydrogen and a water oxygen is narrower, proper to the water molecule. It results in the first maximum of $H-H_W$ in concentrated TBA at 2.6 Å (c_1 in Figure 5a) which resembles that of H_W-H_W in pure water, but shifted upward due to the stronger hydrogen bonding. At the same time, the angular distribution of the hydrogen bond between a water hydrogen and a TBA oxygen is wider, proper to the TBA hydroxyl group. The distribution between the corresponding hydrogens (d_1 in Figure 5a) forms the lower portion below the shoulder of the $H-H_W$ first peak ($g < 0.7$ in Figure 3), coinciding with the ascending slope of the H−H first peak of pure TBA. The correlations between the bonded H of the water and the second nearest TBA neighbors give the second peak of $H-H_W$ (d_2 in Figure 5a) similar to H−H, whereas those of the nonbonded H (c_2 in Figure 5a) make the $H-H_W$ valley at 4 Å shallower than that of H−H. Similar analysis is applicable to the first peak shoulder of the H_W-H_W RDF in concentrated TBA. The only difference is that instead of the valley, the H_W-H_W RDF has a well-pronounced second peak at 4 Å similar to that for the tetrahedral-like hydrogen bonded structure in pure water (Figure 3). This is due to the more directed correlations of a hydrogen bond between two waters (e_2 in Figure 5b).

Water−TBA Hydrophobic Group Correlations. The fist peaks of the C_C−water correlations increase as the TBA concentration rises. Their increase is in accord with the enhancement of the TBA−water and TBA−TBA hydrogen bonding in concentrated TBA solution, and agrees well with the ND data.[17] The agreement, however, is less satisfactory for the C_C-O_W RDF. In the ND results, its first peak splits up into two maxima at 3.6 and 4.8 Å. The former has been attributed to water molecules hydrogen-bonded to the hydroxyl group of TBA (f_1 in Figure 4a), and the latter to the remainder of the TBA hydration shell (f_2 in Figure 4a). Although this splitting feature is barely visible on the broad peak of the C_C-O_W RDF between 3.0 and 5.5 Å obtained in the present calculation, it is reproduced for the C_C-H_W RDF in agreement with the ND data.[17] The experimental C_C-H_W RDF has two peaks at 2.9 and 4.5 Å. The former represents water hydrogens bonded to TBA hydroxyl group oxygen (g_1 in Figure 4a), whereas the latter corresponds to outward hydrogens of waters hydrogen-bonded to TBA (g_2 in Figure 4a) as well as to hydration shell hydrogens around the *tert*-butyl hydrophobic group, oriented preferentially along its surface (g_3 in Figure 4a). It should be noted that the first peak of C_C-H_W is located somewhat too close to C_C with respect to the first peak of C_C-O_W. This drawback and the failure to resolve the splitting of the wide first peak of C_C-O_W can be related to the RISM imperfectness in treatment of auxiliary sites, mentioned before. Nevertheless, this does not violate the qualitative description of the system. The C_C-H_W first peak gets higher with rise of the TBA concentration in agreement with the ND experiment.[17] Furthermore, the calculation correctly reproduces the transition from the tetrahedral-like to zigzag hydrogen-bonding structure of the solution with rise of the TBA concentration, which manifests in the depletion of the second hydration shell peaks of C_C-O_W at 7.0 Å and of C_C-H_W at 7.5 Å (f_3 and g_3 in Figure 4a), and in the rise of the wide and shallow maxima of C_C-O_W and C_C-H_W at a longer-range distance of 10 Å (h_3 and i_3 in Figure 5b).

The ND curve for the $C-O_W$ RDF contains two major peaks at 3.7 and 6 Å, and a small local peak at 5 Å between them.

The first one describes hydration shell water molecules in direct contact with the TBA methyl groups, and the second at 6 Å apparently corresponds to water molecules hydrogen-bonded to the TBA hydroxyl oxygen. This structure is qualitatively reproduced in the calculation, except for the small feature at 5 Å. The latter seems to arise due to the partial charges of the methyl hydrogens, which are omitted in the united-atom model of the methyl group we used at present. There are no striking peaks in the $C-H_W$ RDF, which agrees with the ND results.[17] This indicates the absence of strong orientational ordering of water molecules around the entire *tert*-butyl group of TBA, which is reasonable for hydration of the hydrophobic group. Similarly to the C_C−water correlations, a wide and shallow enhancement of both the $C-O_W$ and $C-H_W$ RDFs at 9 to 10 Å is observed with rise of the TBA concentration, in accord with the ND data.[17]

TBA−TBA Correlations. In the C_C-C_C RDF, the broad first peak at 5.6 Å coincides in position with that observed in the ND data for dilute TBA solutions[17] and pure TBA[18] (Figure 2). It increases and widens with rise of the TBA concentration, which complies with the increase in the C_C-C_C coordination number obtained from the ND data by integrating the C_C-C_C RDF in the first solvation shell.[17,18] It varies from 2.8 at $X_{TBA} = 0.06$ to 5.8 at $X_{TBA} = 0.16$ in dilute TBA solutions[17] up to 10.8 in pure TBA[18] due to widening of the first peak. As the TBA molar fraction rises to pure TBA, a small local maximum at 4.7 Å develops on the ascending slope of the first C_C-C_C peak in the ND data. It is ascribed to the intermolecular correlation through TBA hydrogen bonding.[18] The theory failure to resolve this splitting (Figure 2) is related, as above, to the RISM imperfectness in treatment of the excluded volume for the C_C site buried inside the *tert*-butyl hydrophobic group of TBA.

The second peak of the C_C-C_C RDF for infinite dilution of TBA is obtained at 8.4 Å. With rise of the TBA concentration, the second C_C-C_C peak at 8.4 Å diminishes, whereas another one builds up at 10.7 Å starting from concentrations $X_{TBA} > 0.2$ and increases until $X_{TBA} = 1$. In support of this, the ND data the C_C-C_C RDF displays a similar second peak at about 9 Å in dilute TBA solutions[17] which flattens out at $X_{TBA} = 0.16$ and turns into a wide second maximum at 10 Å in pure TBA[18] (Figure 2). The above modifications of the C_C-C_C RDF accord well with the suggested transition from TBA molecules included into the hydrogen-bonding structure of water to the zigzag-like chains of alcohol as the TBA concentration rises. The first peak of the C_C-C_C RDF corresponds to both the arrangements (distance j_1 in Figure 4b and k_1 in Figure 5a), whereas the second allows one to distinguish between the second nearest TBA neighbors aggregating inside the water tetrahedral-like hydrogen-bonding cage (j_2 in Figure 4b) and ones entering into the zigzag structure of pure alcohol (k_2 in Figure 5a).

The orientational correlation functions obtained from the ND experiment reveal strong intermolecular correlations between the methyl groups of TBA.[18] The behavior of the C−C as well as C_C-C RDFs follow essentially from those of the C_C-C_C correlation discussed above. The first two peaks of C−C at 4 and 6 Å, and of C_C-C at 5 and 7 Å correspond to two *tert*-butyl groups in contact, and give the separations between the methyl groups bonded to C_C at the opposite sides. As the TBA concentration rises, the height of those peaks increases simultaneously with the first peak of the C_C-C_C RDF. Notice also some shift of the first and second peaks to each other for both C−C and C_C-C in concentrated TBA solution. The next peaks of the C−C and C_C-C RDFs displace to larger distance with rise of the TBA concentration, much as the second peak of the C_C-C_C RDF. However, they are much less pronounced in dilute TBA solution because of the varying orientation of TBA molecules bridged by water. The positions of the C−C and C_C-C peaks and their relative shifts with rise of the TBA concentration well coincide with the ND data for pure TBA[18] as well as dilute TBA solutions.[17]

The correlations between the *tert*-butyl and hydroxyl groups of TBA are in agreement with the ND data.[17,18] The C−O RDF contains two major peaks at 3.5 and 6 Å, and a shallow third peak at 8 Å. The only difference consists of the presence of a narrow peak at 5 Å in the ND results for concentrated TBA solutions which apparently corresponds to the all-atom TBA description employed in the ND/EPSR data modeling,[17,18] unlike the united-atom model we use for the methyl groups. The small positive charges of the methyl hydrogen sites result in the local peak of attraction of the negatively charged hydroxyl oxygen of TBA, similarly to the $C-O_W$ RDF discussed before. A similar but much less pronounced feature at 5 Å is lost also on the C_C-O RDF for concentrated TBA. As a major change in the C_C-O RDF with rise of the TBA molar fraction, the theory yields its first peak at 4.1 Å to significantly mount in accord with that at 3.7 Å in the ND data (Figure 2). It is expected that the explicit description of the methyl hydrogens would not modify the C−H and C_C-H RDFs much. The positions of the C−H peaks at 4, 6, and 5 Å and their height change with X_{TBA} comply with the ND data.[17,18] The shoulder of the C_C-H RDF at 2.3 Å in dilute TBA solutions grows into its first peak at 2.3 Å in pure TBA, and the second C_C-H peak at 4.4 Å increases as the TBA molar fraction rises (Figure 2). The position of the first C_C-H peak in pure TBA corresponds to the distance o_1 between TBA neighbors in the zigzag hydrogen-bonding arrangement in Figure 5a. Some discrepancy with its position at 2.9 Å found in the ND experiment[18] is related to the RISM artifact discussed above and does not hamper the qualitative picture of the solvation structure. It should be noted that the first peak of the C_C-H RDF as well as that of C_C-H_W become well-pronounced only in concentrated TBA solution (for $X_{TBA} > 0.4$) where the zigzag hydrogen-bonding structure forms. The second and third C_C-H peak positions at 2.3 and 7.2 Å match the ND experiment[17,18] well. The first and second C_C-O peaks and the second and third C_C-H peaks correspond respectively to distances l_1, l_2, and m_1, m_2 in Figure 4b for a hydrophobic TBA aggregate in water, and to n_1, n_2, and o_2, o_3 in Figure 5a for the zigzag-like hydrogen bonding structure of pure TBA. Notice also the shallow peaks of C_C-O at 9.5 Å and C_C-H at 10 Å in dilute TBA solution (distances l_3 and m_3 in Figure 4b) which flatten out in favor of the even shallower and wider enhancement at about 11 and 12 Å, respectively, in pure TBA (n_3 and o_4 in Figure 5a). They are related to the second-neighbor TBA ordering at distance j_2 in a hydrophobic aggregate, and at k_2 in the zigzag-like hydrogen-bonding structure.

In dilute TBA solution, clustering of TBA molecules is observed. Due to the hydrophobic interaction, they aggregate in arrangements with the nonpolar groups in contact, whereas the TBA−TBA hydrogen bonding does not occur. This trend has been shown in the ND experiment.[18] Although the O−H first peak representing the TBA−TBA hydrogen bonding is quite high even in dilute TBA solution, the small TBA concentration leads to the corresponding coordination number for the hydrogen-bonding peak to be much less than one. The hydrogen-bond sites of TBA molecules are saturated by the neighboring water. On the other hand, the C_C-C_C coordination number for the first peak region amounts to 3 to 6. This value

suggests that TBA molecules aggregate at side-to-side as well as tail-to-tail contact arrangements of their *tert*-butyl groups (at distance j_1 in Figure 4b). The clustered *tert*-butyl groups are surrounded by a hydrogen-bonding cage of water molecules incorporating the hydroxyl groups of aggregated TBA. The side-to-side TBA neighbors are bridged by water molecules rather than directly hydrogen bonded to each other (Figure 4b). Microheterogeneity has been reported also for acetonitrile−water mixtures.[40−42] Since the methyl group in acetonitrile is too small to form aggregations by hydrophobic interaction, it is expected that the acetonitrile molecules aggregate, much as in neat liquid acetonitrile, with a dipole−dipole interaction of CN groups.[42] Because the hydrogen bonding between the acetonitrile CN and water OH groups is weaker than that between OH groups of water, aqueous acetonitrile has large mixing inhomogeneity at last reaching to the phase separation. In contrast, TBA−water hydrogen bonding is as strong as the water one, and so the hydrophobic attraction of the bulky *tert*-butyl groups in aqueous solution forms only small clusters of 3−6 TBA molecules. These findings are consistent with the dynamical properties of TBA−water mixtures. The small diffusion constant in concentrated TBA solutions can be explained by the effectively large mass of the aggregates.[15]

Conclusion

The site−site radial distribution functions of the *tert*-butyl alcohol−water binary mixture have been calculated in the whole concentration range by using the reference interaction site model (RISM) integral equation method. The theory comprises the dielectrically consistent RISM approach developed by Perkyns and Pettitt,[25] and the closure approximation proposed by Kovalenko and Hirata (KH).[26,27] The RISM/KH approximation has been shown to be adequate for treatment of associating molecular fluids in a wide range of density from gas to liquid.[27] In the present context, it provides appropriate description for the association structure in a mixture of polar molecular liquids, which substantially changes with the molar fraction of the constituents. The site−site correlations obtained for the TBA−water mixture are in qualitative agreement with the data available from the small-angle X-ray and neutron diffraction experiments, and the molecular dynamics simulations for dilute aqueous TBA solution and pure TBA liquid. With rise of the TBA concentration, the water−water, TBA−water, and TBA−TBA hydrogen bonds become stronger; however, the water tetrahedral hydrogen-bonding structure is gradually broken. In dilute aqueous TBA solution, aggregates are formed of TBA molecules contacting with each other by the methyl hydrophobic groups, whereas their hydroxyl groups are incorporated into the hydrogen-bonding cage of surrounding water molecules. In concentrated TBA solution, water as well as TBA molecules enter into the zigzag hydrogen-bonding structure typical of alcohol. The present work demonstrates the ability of the RISM/KH theory to predict the salient features of the association structure of alcohol−water liquid mixtures in the whole range of the molar fraction. Since it also yields the thermodynamics of polar molecular fluids,[27] the RISM/KH approach can be further employed in studies of such processes as isomerization and chemical reactions in mixtures of associating molecular liquids.

Acknowledgment. The authors acknowledge the financial support from the Japanese Ministry of Education, Science, Sports, and Culture (Monbukagakusho). K.Y. and T.Y. thank the support from the Joint Study Program (2000−2001) of the Institute for Molecular Science, Okazaki National Research Institutes. A.K. and F.H. thank the Grant-in-Aid from Monbukagakusho for Scientific Research of Priority Areas (B) No. 757 on Nano-Chemistry at Liquid-Liquid Interfaces. The authors are grateful to Dr. Bowron for providing the neutron diffraction experiment results shown in refs 17 and 18.

References and Notes

(1) Franks, F. In *Water Science Reviews*; Franks, F., Ed; Cambridge University Press: New York, 1985; Vol. 1.
(2) Takamuku, T.; Yamaguchi, T.; Asato, M.; Matsumoto, M.; Nishi, N. *Z. Naturforsch.* **2000**, *55a*, 513.
(3) Nishi, N.; Takahashi, S.; Matsumoto, M.; Tanaka, A.; Muraya, K.; Takamuku, T.; Yamaguchi, T. *J. Phys. Chem.* **1995**, *99*, 462.
(4) Matsumoto, M.; Nishi, N.; Furusawa, T.; Saita, M.; Takamuku, T.; Yamagami, M.; Yamaguchi, T. *Bull. Chem. Soc. Jpn*. **1995**, *68*, 1775.
(5) Yamaguchi, T. *Pure Appl. Chem*. **1999**, *71*, 1741 and references therein.
(6) Cinelli, S.; Onori, G.; Santucci, A. *Colloids Surf. A* **1999**, *160*, 3 and references therein.
(7) Nakanishi, K. *Bull. Chem. Soc. Jpn.* **1960**, *33*, 793.
(8) Roux, G.; Roberts, D.; Peron G.; Desnoyer, J. E. *J. Solution Chem.* **1980**, *9*, 629.
(9) Nishikawa, K.; Kodera, Y.; Iijima, T. *J. Phys. Chem*. **1987**, *91*, 3694.
(10) Nishikawa, K.; Hayashi, H.; Iijima, T. *J. Phys. Chem*. **1989**, *93*, 6559.
(11) D'Arrigo, G.; Teixeira, J. *J. Chem. Soc., Faraday Trans*. **1990**, *86*, 1503.
(12) Freda, M.; Onori, G.; Santucci, A. *J. Phys. Chem. B* **2001**, *105*, 12714.
(13) Onori, G.; Santucci, A. *J. Mol. Liq.* **1996**, *69*, 161.
(14) Nakanishi, K.; Ikari, K.; Okazaki S.; Touhara, H. *J. Chem. Phys.* **1984**, *80*, 1656.
(15) Tanaka H.; Nakanishi K.; Touhara H. *J. Chem. Phys*. **1984**, *81*, 4065.
(16) Kusalik, P. G.; Lyubartsev, A. P.; Bergman, D. L.; Laaksonen, A. *J. Phys. Chem. B* **2000**, *104*, 9526; 9533.
(17) Bowron, D. T.; Finney, J. L.; Soper, A. K. *J. Phys. Chem. B* **1998**, *102*, 3551.
(18) Bowron, D. T.; Finney, J. L.; Soper, A. K. *Mol. Phys.* **1998**, *93*, 531.
(19) Soper, A. K. *Chem. Phys.* **1996**, *202*, 295.
(20) Hansen, J. P.; McDonald, I. R. *Theory of Simple Liquids*, 2nd ed.; Academic: London, 1986.
(21) Chandler, D.; Andersen, H. C.*J. Chem. Phys.* **1972**, *57*, 1930.
(22) Chandler, D. *J. Chem. Phys.* **1973**, *59*, 2749.
(23) Hirata, F.; Pettit, M.; Rossky, P. J. *J. Chem. Phys.* **1982**, *77*, 509.
(24) Hirata, F. *Bull. Chem. Soc. Jpn.* **1998**, *71*, 1483.
(25) Perkyns, J. S.; Pettitt, B. M. *J. Chem. Phys.* **1992**, *97*, 7656.
(26) Kovalenko, A.; Hirata, F. *J. Chem. Phys.* **1999**, *110*, 10095.
(27) Kovalenko, A.; Hirata, F. *Chem. Phys. Lett.* **2001**, *349*, 496.
(28) Tanaka, H.; Walsh, J.; Gubbins, K. E. *Mol. Phys.* **1992**, *76*, 1221.
(29) Kubota, H.; Tanaka, Y.; Makita, T. *Int. J. Thermophys.* **1987**, *8*, 47.
(30) Broadwater, T. L.; Kay, R. L. *J. Phys. Chem.* **1970**, *74*, 8802.
(31) Berendsen, J. C.; Crigera, J. R.; Straatsma, T. P. *J. Phys. Chem.* **1987**, *91*, 6269.
(32) Pettitt, B. M.; Rossky, P. J. *J. Chem. Phys.* **1982**, *77*, 1451.
(33) Maw, S.; Sato, H.; Ten-no, S.; Hirata, F. *Chem. Phys. Lett*. **1997**, *276*, 20.
(34) Jorgensen, W. L. *J. Phys. Chem*. **1986**, *90*, 1276.
(35) Talman, J. D. *J. Comput. Phys.* **1978**, *29*, 35.
(36) Rossky, P. J.; Friedman, H. L. *J. Chem. Phys.* **1980**, *72*, 5694.
(37) Kovalenko, A.; Hirata, F. *J. Chem. Phys.* **2000**, *112*, 10391.
(38) Kovalenko, A.; Ten-no, S.; Hirata, F. *J. Comput. Chem.* **1999**, *20*, 928.
(39) Kovalenko, A.; Hirata, F. *J. Phys. Chem. B* **1999**, *103*, 7942.
(40) Kovacs, H.; Laaksonen, A. *J. Am. Chem. Soc*. **1991**, *113*, 5596.
(41) Bergmann, D. L.; Laaksonen, A. *Phys. Rev. B* **1998**, *58*, 4706.
(42) Nishikawa, K.; Kasahara, Y.; Ichioka, T. *J. Phys. Chem. B* **2002**, *106*, 693.